

1 **Modeling the influence of moulin shape on subglacial**
2 **hydrology**

3 **Celia TRUNZ^{1,2}, Matthew D. COVINGTON¹, Kristin POINAR³,**
4 **Lauren C. ANDREWS⁴, Jessica MEJIA^{3,5}, Jason GULLEY⁵**

5 ¹Geosciences Department, University of Arkansas, Fayetteville AR, USA

6 ²Department of Applied Geomatics, Université de Sherbrooke, Sherbrooke QC, CA

7 ³Department of Geology, University at Buffalo, Buffalo NY, USA

8 ⁴Global Modeling and Assimilation Office, NASA Goddard Space Flight Center, Greenbelt MD, USA

9 ⁵Geosciences Department, University of South Florida, Tampa FL, USA

10 **Key Points:**

- 11 • We use a single-channel subglacial hydrological model to study how moulin size
12 and shape affect subglacial water pressure.
- 13 • Subglacial water pressure dynamics are controlled by the moulin cross-sectional
14 area only within the range of daily water level oscillations.
- 15 • Storage parameters meant to represent moulins in hydrologic models need to rep-
16 resent dynamic storage near equilibrium head elevations.

Abstract

18
19
20
21
22
23
24
25
26
27
28
29
30
31
32
33

Subglacial models represent moulins as cylinders or cones, but field observations suggest the upper part of moulins in the Greenland Ice Sheet have more complex shapes. These more complex shapes should cause englacial water storage within moulins to vary as a function of depth, a relationship not currently accounted for in models. Here, we use a coupled englacial–subglacial channel model to explore how moulin shape affects depth-dependent moulin water storage and water pressure dynamics within a subglacial channel. We simulate seven different moulin shapes across a range of moulin sizes. We find that the englacial storage capacity at the water level is the main control over the daily water level oscillation range and that depth-varying changes in englacial water storage control the temporal shape of this oscillation. Further, the cross-sectional area of the moulin within the daily oscillation range, but not above or below this range, controls pressures within the connected subglacial channel. Specifically, large cross-sectional areas can dampen daily to weekly oscillations that occur in the surface meltwater supply. Our findings suggest that further knowledge of the shape of moulins around the equilibrium water level would improve englacial storage parameterization in subglacial hydrological models and aid predictions of hydrodynamic coupling.

34

Plain Language Summary

35
36
37
38
39
40
41
42
43

The speed of glacier ice flowing towards the ocean is influenced by timing and the amount of water flowing in moulins. Moulins are large vertical shafts that penetrate the entire ice thickness to transport water from the glacier’s surface to the bed. Water levels within moulins reflect the water pressure within channels that form underneath the glacier, transporting meltwater seaward. Most models that are used to simulate this water flow under the ice assume that moulins are cylindrical, but in reality they are not. In this study, we show that non-cylindrical moulins affect how the water level fluctuates within moulins, and that what matters is the shape of the moulin within the range where the water level oscillates.

44

1 Introduction

45
46
47
48
49
50
51
52

In land-terminating regions of the Greenland Ice Sheet, the response of the subglacial drainage system to meltwater inputs is a primary influence on ice motion (e.g., Andrews et al., 2014; Hoffman et al., 2016; Schoof, 2010). Spatial (Banwell et al., 2016) and temporal (Schoof, 2010) variability in supraglacial meltwater input affects subglacial channel water pressures and ice motion. While pressures within subglacial channels tend to control mid-melt-season ice motion, changes in the inefficient subglacial drainage system can influence late-season slowdowns (Andrews et al., 2014; Hoffman et al., 2016; Mejia et al., 2021).

53
54
55
56
57
58
59

Englacial storage exerts an important control on the pressure dynamics within the subglacial drainage system (Flowers & Clarke, 2002). Storage must be included within some subglacial models to produce realistic oscillation dynamics in channelized subglacial drainage systems (Werder et al., 2013). Storage can affect both the distance over which pressure variations will diffuse away from channels (Werder et al., 2013) and the rate of water pressure rise after the melt season (Downs et al., 2018). Consequently, storage plays a central role in the link between meltwater and ice motion.

60
61
62
63
64

Moulins collect nearly all of the supraglacial meltwater on the Greenland Ice Sheet (Smith et al., 2015) and route this meltwater to the most efficient parts of the subglacial drainage system (Gulley et al., 2012). By connecting to subglacial channels, subglacial water pressures are modulated by the water stored within moulins (Banwell et al., 2016; Werder et al., 2013). Moulins represent a potentially large percentage of the englacial

void space that is directly coupled to the subglacial system (Covington et al., 2020). Most subglacial hydrological models treat englacial storage as a spatially uniform and temporally constant model parameter, such as englacial void fraction (Bartholomäus et al., 2011; Hewitt, 2013; Hoffman et al., 2016; Koziol & Arnold, 2018; Stevens et al., 2018; Sommers et al., 2018; Werder et al., 2013). However, limited exploration within moulines in alpine type glaciers (e.g. Gulley et al., 2009; Holmlund, 1988; Vallot, 1898; Vatne & Irvine-Fynn, 2016) and in Greenland (Bourseiller et al., 2002; Covington et al., 2020; Griselin, 1995; Lamberton, 2002; Moreau, 2009) suggests that moulines often have irregular shapes, where storage capacity varies substantially with depth.

In this study, we explore how moulin shape affects water level dynamics in moulines and subglacial channels in settings similar to the ablation zone of the Western Greenland Ice Sheet using the single-channel model developed by Covington et al. (2020). Since relatively little is known about specific moulin shapes in Greenland, we explore a variety of generic shapes and discuss how they relate to field observations. In Section 3.1, we explore how various moulin shapes affect the dynamic timescales of the subglacial system using a constant meltwater input to the moulin. In Section 3.2, we test how the shape of a moulin affects its response to diurnally varying meltwater input. We conclude by interpreting our simulation results in the context of the englacial void ratio, bed connectivity, and consequent ice velocity.

2 Model description

Diameter-evolving subglacial channels have been simulated in numerous prior studies (e.g. Röthlisberger, 1972; Schoof, 2010; Spring & Hutter, 1981) and can be coupled with a reservoir to include the storage of the moulin (Clarke, 1996; Covington et al., 2012; Werder et al., 2010). This type of model provides a simple and efficient physically based framework for studying the dynamics of an individual moulin-fed subglacial channel.

To explore the relationship between moulin shape and moulin water level variation, we employ a simplified model of the coupled englacial-subglacial hydrological system. The model is a 0D model and contains a single subglacial channel that is fed by a vertical moulin (Figure 1a). The moulin collects meltwater input which is then evacuated through a subglacial channel. The moulin’s shape remains fixed throughout any single model run, with only the subglacial channel’s cross-sectional area (S) allowed to evolve through melt and creep (Figure 1b), which are functions of subglacial discharge and effective pressure, respectively. Discharge and effective pressure vary with the height of the water column within the moulin’s shaft, which we represent as hydraulic head (h). The rate of change of head (dh/dt) depends on the difference between the discharge into (Q_{in}) and out of (Q_{out}) the moulin and the storage volume within the moulin. Importantly, storage is controlled by the cross-sectional area of the moulin at the water level, $A_r(h)$.

2.1 Model structure

For this study, we implement the reservoir constriction model described in Covington et al. (2012) with the subglacial channel evolution model described in Schoof (2010), without the cavity component, as we assume the subglacial system is already channelized. The moulin component was adapted to allow the moulin cross-sectional area (A_r) to vary with depth. The model is composed of two coupled ordinary differential equations simulating the time evolution of moulin head (h) and the subglacial channel cross-sectional area (S) at the entrance of the channel where the water exits the moulin. The rate of change of head (h) within the moulin is given by

$$\frac{dh}{dt} = \frac{1}{A_r(h)} (Q_{\text{in}} - Q_{\text{out}}), \quad (1)$$

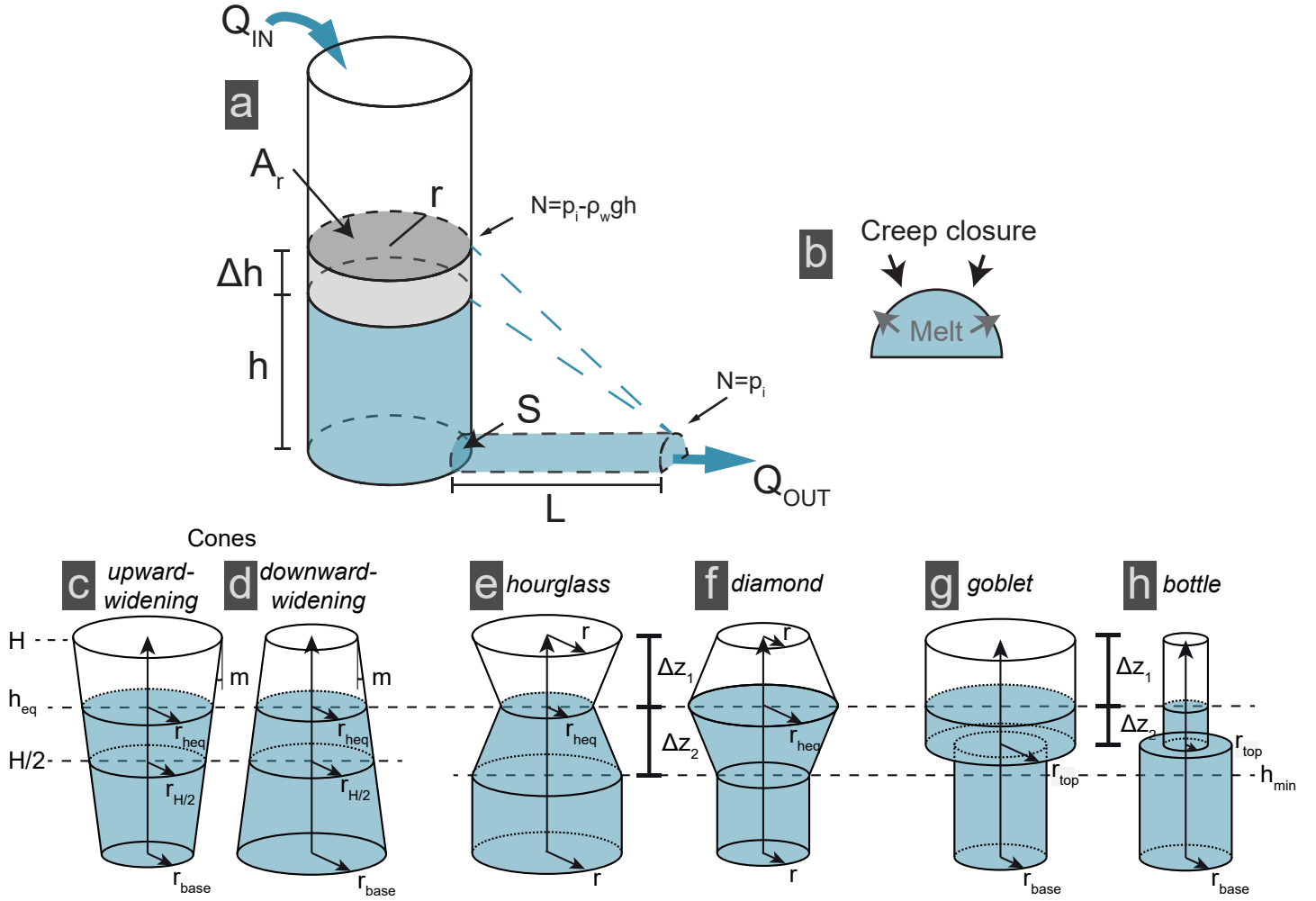


Figure 1. Schematic model diagrams. (a) Sketch of the model representing a moulin connected with a subglacial channel (Covington et al., 2012), with the meltwater input (Q_{in}), discharge (Q_{out}), moulin cross-sectional area (A_r), moulin radius (r), moulin head (h), subglacial channel length (L), and subglacial channel cross-sectional area (S). The effective pressure (N) in the subglacial channel in the vicinity of the moulin is the pressure of the ice (P_i) minus the pressure of the water ($\rho_w g h$) defined with the water density (ρ_w), the gravity (g) and the head (h) relative to the bed. The blue dashed line represents the hydraulic gradient. Water pressure is zero at the output of the subglacial channel (b) The subglacial channel can creep closed or open depending on head and ice thickness (adapted from Schoof (2010)) (c-d) Cone-shaped moulin used for constant meltwater input simulations. We compare different cones by fixing the radius at the equilibrium head (h_{eq}) or at half of the ice thickness ($H/2$). The slope of the moulin wall is determined by m and is described in more detail in Supporting Text S2. (e-f) Moulin shapes designed so that the change in wall slope is fixed at h_{eq} . (g-h) Moulin shapes with an abrupt change in radius between h_{min} and h_{eq} .

113 where $A_r(h)$ is the cross-sectional area A_r of the moulin at h , Q_{in} is the meltwater in-
 114 put into the moulin, and Q_{out} is the subglacial channel water output. Following Schoof
 115 (2010), we invoke the Darcy-Weisbach equation,

$$116 \quad Q_{\text{out}} = C_3 S^{5/4} \sqrt{\rho_w g h / L}, \quad (2)$$

117 where L is the channel length or, equivalently, the distance between the moulin and the
 118 ice-sheet margin for this simplified case of a single subglacial channel, ρ_w is the water
 119 density, g is the gravitational acceleration. The friction parameter $C_3 = 2^{5/4} \sqrt{\pi} / (\pi^{1/4} \sqrt{\pi + 2\sqrt{\rho_w f}})$,
 120 where f is the Darcy-Weisbach friction factor. The coupled subglacial channel creep and
 121 melt equations are based on the Röthlisberger (1972) and Nye (1976) description of R-
 122 channels and are given by

$$123 \quad \frac{dS}{dt} = C_1 C_3 S^{5/4} \left(\frac{\rho_w g h}{L} \right)^{3/2} - C_2 (P_i - \rho_w g h)^n S. \quad (3)$$

124 The melt opening parameter $C_1 = 1/(\rho_i L_f)$, where L_f is the latent heat of fusion, and
 125 ρ_i is ice density. The viscous creep closure parameter is $C_2 = 2Bn^{-n}$, where B is the
 126 Glen's law fluidity coefficient and n is the Glen's law exponent. The ice overburden pres-
 127 sure is $P_i = \rho_i g H$, where H is the ice thickness.

128 The model makes the following assumptions (Figure 1): (1) bed slope is zero; (2)
 129 the hydraulic gradient in the channel is controlled by the large-scale ice sheet topogra-
 130 phy, thus, prescribing $h = 0$ at the margin, it is defined as $-h/L$; and (3) melt and creep
 131 dynamics within the channel are controlled by the water pressure and ice thickness in
 132 the vicinity of the moulin; (4) water flow in the subglacial channel is turbulent; and (5)
 133 water that enters the moulin leaves only through the subglacial channel. For simplicity,
 134 we consider that all of the water transits through the channel; we do not account for loss
 135 or exchange of water with the distributed or weakly connected parts of the subglacial
 136 system. The model is a 0-D or lumped model, therefore, the cross-sectional area of the
 137 subglacial channel is represented by a single value.

138 Our model is a simplification of one part of the full subglacial hydrological system
 139 and cannot capture the spatial evolution of water pressure along a subglacial channel.
 140 However, it contains all of the components required to explore relationships between moulin
 141 storage and pressure variability in the subglacial channel in the vicinity of the moulin
 142 without introducing unnecessary complexity and uncertain parameters. A variety of sim-
 143 ilar lumped models have been used in previous studies (Arnold et al., 1998; Bartholomew
 144 et al., 2012; Clarke, 1996; Covington et al., 2012, 2020; Cowton et al., 2016; Dow et al.,
 145 2014; Schoof, 2010; Stubblefield et al., 2019; Werder et al., 2010). Specifically, Stubblefield
 146 et al. (2019) demonstrated that such a lumped model displays very similar dynamics to
 147 a more complex extended channel model. We also test this assumption with a simula-
 148 tion comparing our simple 0-D model to an extended 1-D channel model (supporting Text
 149 S3 and Figure S6). Limitations of our simplified modeling approach are discussed in more
 150 detail in Section 4.2.

151 2.2 Boundary conditions and parametrization

152 We use meltwater input rates in the range of estimated supraglacial stream discharges
 153 in the ablation zone on the western flank of the Greenland Ice Sheet (Smith et al., 2015).
 154 We run two broad types of simulations. In the first type of simulations (Section 3.1), the
 155 meltwater input Q_{in} is fixed at $3 \text{ m}^3 \text{ s}^{-1}$ to test the equilibration of the subglacial sys-
 156 tem in the case of an abrupt change in meltwater input conditions, free of the diurnal
 157 variations typical of field-observed supraglacial discharge. This isolates the internal sys-
 158 tem dynamics from any effects of time-varying forcing. In the second type of simulations
 159 (Section 3.2–3.3), we use diurnally varying supraglacial meltwater input:

$$160 \quad Q_{\text{in}}(t) = Q_a \sin(2\pi t/P) + Q_{\text{mean}}, \quad (4)$$

161 where Q_{in} is meltwater input rate in function of time (t). Q_{in} oscillates around a mean
 162 meltwater input $Q_{\text{mean}} = 3 \text{ m}^3 \text{ s}^{-1}$ with an amplitude (Q_{a}) of $0.4 \text{ m}^3 \text{ s}^{-1}$ and a period
 163 (P) of one day. This diurnal range of moulin input is kept low to prevent the simulated
 164 water level from overflowing. The simulations are run for an initialization stage of 40 days,
 165 until the amplitude of the daily oscillations stabilizes. This allows us to isolate the dy-
 166 namics created by varying meltwater input, rather than the damped oscillations produced
 167 during the equilibration of the system.

168 For most of the simulations (Section 3.1.1, 3.2 –3.3), we use a single ice thickness
 169 of 1000 m, which is appropriate for a moulin 30 km away from the margin, to simulate
 170 moulins located within a single area of the ice sheet. We choose parameter values that
 171 are roughly representative of the field areas in Greenland where moulin water-level data
 172 are available (Andrews et al., 2014; Covington et al., 2020). By keeping the ice thick-
 173 ness constant across simulations, we are able to isolate the influence of different moulin
 174 shapes and meltwater input magnitudes on moulin water level and subglacial water pres-
 175 sures. For the simulations in Section 3.1.2, however, we test how the system behaves at
 176 different positions across the ice sheet. In order to scale the ice thickness at the moulin
 177 to a series of channel lengths representative of the profile of a land-terminating glacier
 178 in Greenland, we use an idealized square root glacier (Hewitt et al., 2012), with zero ice
 179 thickness at the margin and 1000 m ice thickness at 30 km from the margin, defined by

$$180 \quad H = \sqrt{\frac{L}{30}}, \quad (5)$$

181 where H is the ice thickness and L is again the subglacial channel length, equivalent to
 182 the distance between the moulin and the margin. This equation provides a single value
 183 of ice thickness in the vicinity of the moulin for each simulation with a given distance
 184 from the margin.

185 To explore the influence of moulin shape on subglacial water pressure dynamics,
 186 we use a series of idealized moulin shapes with geometries illustrated in Figure 1c–h. These
 187 shapes were chosen to cover a wide spectrum of possible moulin geometries because, to
 188 date, shapes of Greenland moulins have not been mapped at depths representative of
 189 summer water level oscillation ranges. We adapt the model of Covington et al. (2012)
 190 (Figure 1) by implementing a moulin with circular cross-sectional area $A_r = \pi r^2$, for
 191 a depth-dependent radius r (Clarke, 1996; Werder et al., 2010). The slope of the wall
 192 (m) is defined as $m = dr/dz$, where r is the moulin radius and z the elevation from the
 193 bed.

194 2.3 Types of simulation sets

195 We produce different simulation sets, depending on the type of meltwater inputs
 196 and position on the ice sheet (Table 1. For each simulation set, we compare moulins of
 197 different sizes and shapes with identical radii either at the elevation of half of the ice thick-
 198 ness ($H/2$) or at the equilibrium head (h_{eq}), which is the head at which the water level
 199 in the moulin would stabilize under constant discharge (Röthlisberger, 1972), approx-
 200 imated to the average discharge in the case of oscillating meltwater input. In the first
 201 set, the simulations (Section 3.1.1) are run with fixed meltwater inputs at one position
 202 on the ice sheet, and in the second set (Section 3.1.2) the simulations are run at several
 203 positions along a transect. For both simulation sets, we compare simulation subsets made
 204 with cylindrical, cone-shaped, and “diamond” moulins (Figure 1e–f) of different sizes and
 205 wall slopes but identical radii at h_{eq} or identical radii at $H/2$. The parameterization is
 206 described in Supporting Text S2. In the third set (Section 3.2) the simulations are run
 207 with an oscillating meltwater input. For this simulation set, we compare cylindrical, “hour-
 208 glass”, and “diamond”, -shaped moulins (Figure 1c–f) to test how the change of slope
 209 influences the moulin head dynamics. The parameterizations of moulin shapes are de-
 210 scribed in the Supporting Information (Figure S5). In the fourth set (Section 3.3) the

Table 1. Summary of the simulation sets.

Section	H (m)	L (m)	Q_{in}	Shapes
3.1.1	1'000	30'000	constant	cylindrical, conical, diamond, hourglass
3.1.2	equation 5	0–40'000	constant	cylindrical, conical, diamond, hourglass
3.2	1'000	30'000	oscillating	cylindrical, diamond, hourglass
3.3	1'000	30'000	constant & oscillating	cylindrical, bottle, goblet

simulations are run both with a constant input and an oscillating meltwater input. For this simulation set, we compare “goblet”, and “bottle”-shaped moulin (Figure 1g–h), to test how an abrupt change in cross-sectional area influences moulin head dynamics.

3 Model experiments

3.1 Model experiments with a fixed meltwater input

For a fixed rate of meltwater discharge within a subglacial channel, there exist equilibrium values for head (h_{eq}) and channel cross-sectional area (S_{eq}) that can accommodate this discharge while simultaneously balancing the rates of wall melt and creep closure within the channel (Röthlisberger, 1972). If a channel is initialized at this state, then it will remain at equilibrium until the external forcing changes. When a subglacial channel is coupled to an englacial storage element, such as a moulin, the system can spontaneously oscillate around these values of equilibrium head and diameter, even with constant meltwater delivery (Clarke, 1996; Stubblefield et al., 2019). However, for the parameter space that we explore here, if our model is run with constant discharge and initialized sufficiently far from the equilibrium head and channel diameter for that discharge, then it behaves as a damped oscillator, which eventually approaches the equilibrium state (Supporting Figure S1). Therefore, the system exhibits two inherent dynamic timescales (Supporting Figure S1): an oscillation timescale (τ_{osc}) and a damping timescale (τ_{damp}), the latter of which is an equilibration timescale represented by the e-folding time over which the the oscillations decay by a factor of e. Effectively, τ_{damp} approximates the time that is required for the system to evolve from one equilibrium state to another after a change in forcing, such as the moulin discharge. We calculate the value of (h_{eq}) for each simulation using the root-finding function “*solve_ivp*” from the *scipy* package in Python, and we run simulations with initial values of 110% h_{eq} and S_{eq} . We determine τ_{osc} and τ_{damp} by fitting our simulated moulin head timeseries to the damped harmonic oscillator function

$$h(t) = ae^{-t/\tau_{\text{damp}}} \sin\left(\frac{2\pi}{\tau_{\text{osc}}}t + \phi\right) + h_{\text{eq}} \quad (6)$$

$$\phi = \begin{cases} \pi & \text{if } h(t=0) < h_{\text{eq}} \\ 0 & \text{if } h(t=0) > h_{\text{eq}} \end{cases} \quad (7)$$

where a is the amplitude, ϕ is the phase shift, and t is the time of the simulated time-series. We fit the four parameters τ_{osc} , τ_{damp} , a , and ϕ , using a non-linear least-square fit function “*curve_fit*” from the *scipy* package in Python. Because the initial conditions and the forcing can influence the absolute value of the simulation results and the timescales, we systematically use the same boundary condition Q_{in} , and the initial head h_0 and initial subglacial cross-sectional area S_0 , to enable comparison between the simulations.

Here, we run two sets of constant meltwater input simulations. In the first set, we fix parameters of ice thickness and channel length and explore the impact that moulin shape has on the dynamic timescales (Section 3.1.1). In the second simulation set, we systematically vary ice thickness and channel length for a subset of possible moulin shapes

249 (Section 3.1.2). We use this second set of simulations to examine whether sensitivity to
250 moulin shape varies across the ice sheet.

251 3.1.1 Effect of moulin shape on dynamic timescales

252 First, we examine the impact of moulin shape on dynamic timescales for fixed ice
253 thickness and channel length. We run four subsets of simulations using four different meth-
254 ods for varying moulin shapes. For the first subset, we use cylindrical moulins and sim-
255 ply vary the moulin radius from 5 to 15 m (Figure 2 a–c), which is in the range of radii
256 observed in the field by (Covington et al., 2020). In the other three simulation subsets,
257 we use moulins with sloping walls that widen either upward or downward. For the sec-
258 ond subset, we employ a common moulin radius of 10 m at $H/2$ (Figure 2 d–f). For the
259 third and fourth simulation subset, we fix the moulin radius to 10 m at h_{eq} (Figure 2 g–
260 l). For the fourth simulation subset (Figure 2 j–l), however, we mirror the moulin shape
261 around h_{eq} so that the radius at h_{eq} is either the smallest or the largest within the range
262 of water level oscillations. The wall slope, m , ranges from -2% to $+2\%$ for the simula-
263 tions with a common radius at $H/2$, and from -6% to $+6\%$ for the simulations with a
264 common radius at the equilibrium head elevation.

265 In the four subsets of simulations shown in Figure 2, the head (h) and subglacial
266 cross-sectional area at the moulin’s outlet (S) have underdamped oscillations. For all the
267 simulations, the head reaches an equilibrium at about 750 m above the bed. For the cylin-
268 drical subset (Figure 2a–c), we observe that, for the same Q_{in} of $3\text{ m}^3\text{ s}^{-1}$, head oscilla-
269 tions in the larger moulin ($r = 15\text{ m}$) decay with a damping timescale of 10 days and
270 have an oscillation period of five days (Supporting Table S4). The damping time for the
271 decay of oscillations in the smaller moulin ($r = 5\text{ m}$) is about one day with an oscilla-
272 tion period of less than two days (Supporting Tables S2–S4). This is consistent with com-
273 mon reservoir-model behavior, wherein the timescale for filling and draining increases
274 with increasing reservoir size (e.g., Covington et al., 2009, 2012; Stubblefield et al., 2019).

275 In the simulation subset with cone-shaped moulins with radius fixed at $H/2$ (Fig-
276 ure 2d–f) the shapes and total volumes of the moulins are quite different than for the
277 cylindrical cases. However, they display behavior that is similar to the cylindrical cases.
278 For example, an upward-widening cone with wall slope of $+2\%$ from the vertical axis (pur-
279 ple line) has a low total storage capacity below the water line compared to a downward-
280 widening cone with the opposite wall slope (-2% ; red line). However, we observe very
281 similar behavior in the time evolution of h and S as for cylindrical moulins, where equi-
282 libration time increases with moulin storage volume within the range of water level oscil-
283 lation. We probe this further using the third and fourth subset of modeled moulins,
284 where storage at h_{eq} is fixed with a radius of $r = 10\text{ m}$ (Figure 2g–i and j–l). For the
285 third subset (Figure 2g–i), we observe that the timescales of both oscillation and equi-
286 libration are nearly identical from one moulin to another, regardless of wall slope. This
287 is true even for extreme cases of wall slope (Figure 2g–i, red and purple lines). Both h
288 and S vary nearly identically as in the cylindrical (2c, black line) and cone $H/2$ (2f, black
289 line) cases that have $r = 10\text{ m}$ at h_{eq} . We observe a similar behavior for the fourth sub-
290 set (Figure 2j–l), with a bit more variation in the dynamic timescales between the dif-
291 ferent simulations than for the cone-shaped moulins. The mirroring of the slope above
292 and below h_{eq} increases the effect of wall slopes, since the change in area is either pos-
293 itive or negative during both high and low water. For the conical moulins, the opposite
294 signs of the changes in area above and below equilibrium have a cancelling effect.

295 While the dynamic timescales are effectively the same for all the simulations with
296 similar $r(h_{\text{eq}})$, the shape of the oscillations near the peaks and the troughs depends on
297 wall slope (Figure 2g–i). The shape of the head extremum is rounder in Figure 2g (pur-
298 ple line) when the moulin widens in the direction of head displacement (red line), and
299 more sharply peaked when the moulin narrows in that direction.

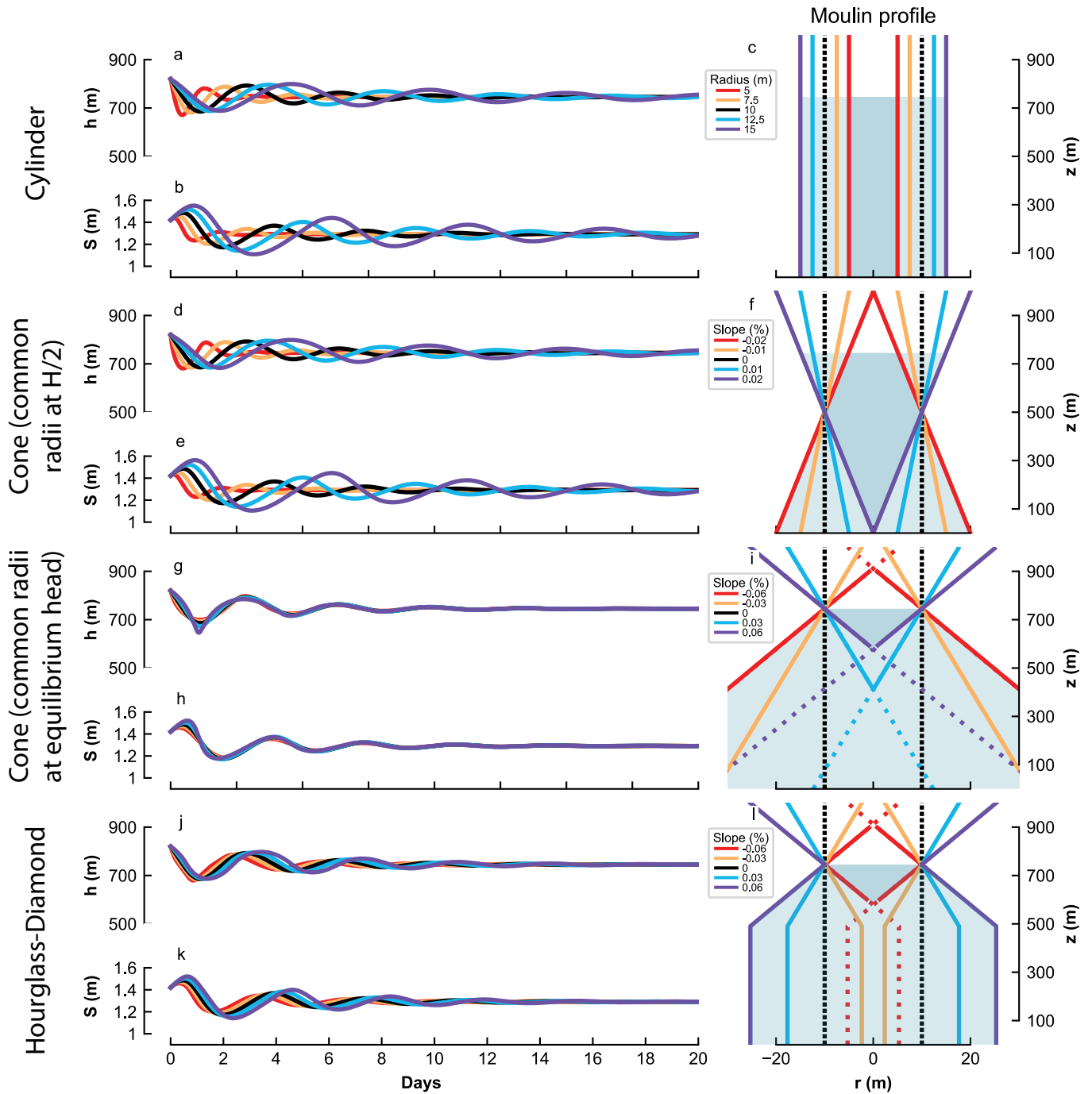


Figure 2. Equilibration timeseries of head (h) and channel cross-sectional area (S) simulated with a fixed meltwater input Q_{in} for various moulin shapes. For all simulations the length and thickness of the glacier are constant. Rows correspond to the following moulin shapes: cylindrical (a–c) with variable diameters, conical (d–i) with variable wall slopes with the radius held constant at an elevation of half the ice thickness (d–f) or at the equilibrium head altitude (g–i), and hourglass-diamond (j–l) centered around the equilibrium head altitude. For each shape, the timeseries of moulin head ($h(m)$) and subglacial channel cross-sectional area (S) are shown on the left. The moulin’s cross-sectional profile is on the right with dark blue and light blue illustrating water common to all moulins and water in a subset of moulins, respectively. The vertical axes of moulin profiles are at scale with head, but not with S . Model parameters are $Q_{in} = 3 \text{ m}^3 \text{ s}^{-1}$, $L = 30 \text{ km}$, $H = 1000 \text{ m}$.

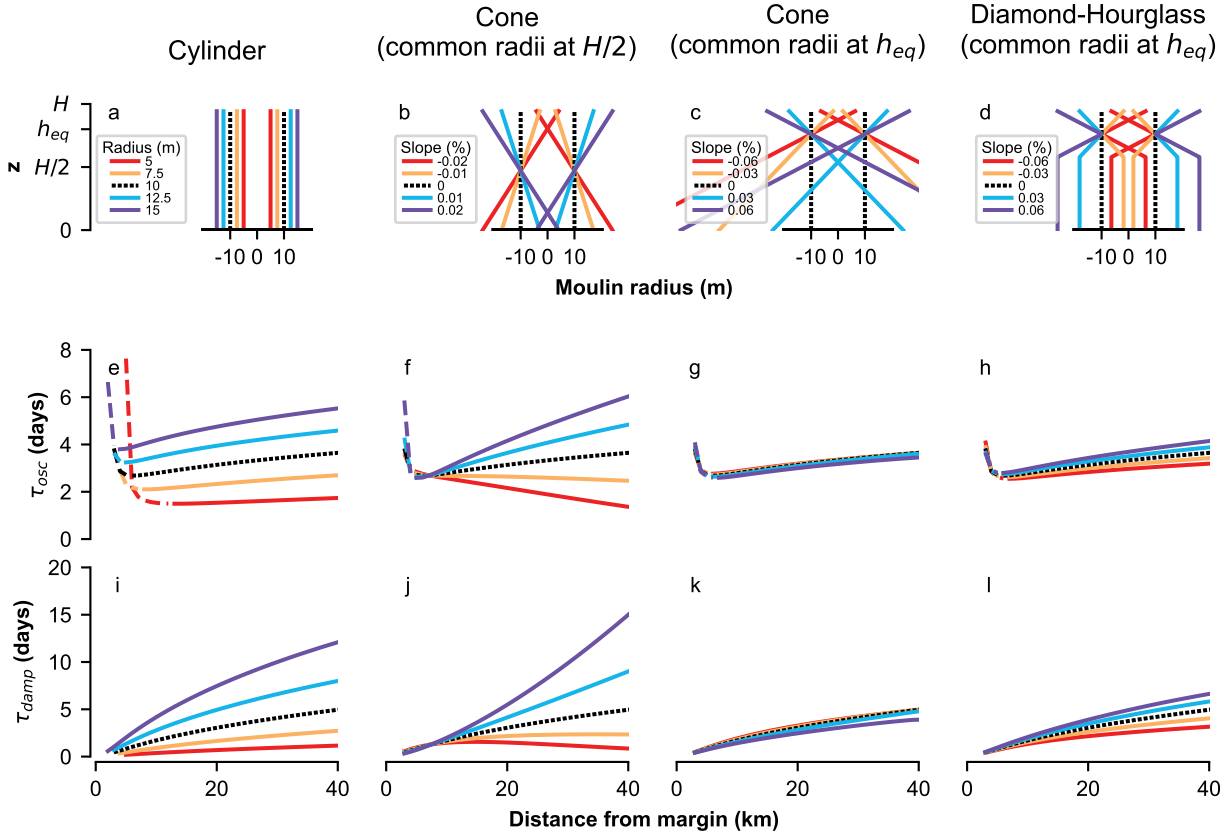


Figure 3. The dynamic timescales (oscillation timescale, τ_{osc} , and damping timescale, τ_{damp}), along an idealized parabolic ice sheet profile (Equation 5), for a cylindrical moulin (left column), cone-shaped moulins with either a fixed radius at $H/2$ (second column) or at h_{eq} (third column), and diamond-hourglass shaped moulins with a fixed radius at h_{eq} (right column). Dashed lines represent simulation results where the head reached equilibrium before a full oscillation cycle (see Supporting Figure S8).

3.1.2 Dynamic timescales for different ice thicknesses

300

301 To examine if the dynamic timescales are sensitive to the moulin position on the
 302 ice sheet, we run a series of simulations representing every 1 km along a 40 km profile of
 303 an idealized parabolic glacier (Figure 3) by systematically varying the parameters of H
 304 at the moulin and L from the moulin to margin. As before, each of these simulations uses
 305 a single ice thickness representative of the ice thickness near the moulin. The idealized
 306 glacier shape is only used to appropriately scale ice thickness at the moulin with distance
 307 from the margin. We use the same four classes of moulin shapes as in Section 3.1.1. For
 308 each shape class we compare the dynamic timescales τ_{osc} and τ_{damp} .

309 For cylindrical moulins with the same meltwater input (Q_{in}), we find that oscil-
 310 lation and damping timescales (τ_{osc} and τ_{damp}) increase with distance from the margin
 311 and with increasing radius (Figure 3, first column). Note that τ_{osc} in (Figure 3e–h) has
 312 high values close to the margin, where the damping of the head towards equilibrium is
 313 quicker than a full period of oscillation (see Supporting Figure S8). Consequently, we
 314 are unsure how physically meaningful the fitting method is for finding the oscillation timescale
 315 close to the margin. For cone-shaped moulins with common radii at $H/2$ (Figure 3, sec-

ond column), the timescales display an intersection point around 10 km from the margin, a distance that is specific to our parameter choices. Here, for downward-widening moulins, the timescales initially decrease with distance from the margin, because increases in the equilibrium head bring the water levels into a narrower portion of the moulin. For upward-widening moulins a similar, but opposite effect produces increases in the timescales with distance from the margin. As a result, for a wall slope of 0.02, τ_{damp} reaches a maximum of 15 days at 40 km, where the moulin radius at the water level becomes disproportionately large compared to the meltwater input. Overall, these results illustrate that the diameter of the moulin at h_{eq} is the primary control on these timescales and that channel melt and creep dynamics have a secondary effect. This is further demonstrated by the simulations for cone-shaped and diamond-hourglass moulins with common radii at h_{eq} (Figure 3 right columns), which show reduced variation in τ_{osc} and τ_{damp} across moulin shapes, so long as the radius at h_{eq} is the same.

For the simulations with common radii at h_{eq} , both timescales reflect mainly the position of the moulin on the ice sheet, not the moulin shape. Furthermore, τ_{osc} and τ_{damp} for all cone-shaped moulins in this subset are the same as that of the cylindrical moulin with a radius of 10 m, which is equal to the radius of the cone-shaped moulins at h_{eq} . Therefore, we find that the moulin’s cross-sectional area at h_{eq} controls the dynamic timescales.

3.2 Model experiments with an oscillating meltwater input

On glaciers and ice sheets, meltwater discharge flowing into moulins is not constant in time but oscillates with changes in surface melt. In this section, we focus on the impact of moulin shape on the dynamics of moulin water level and subglacial channel cross-sectional area under diurnally varying meltwater delivery.

We test a variety of simple, physically plausible shapes. We design these moulins such that the changes in cross-sectional area are focused within the range of elevations of water level oscillation, since results in Section 3.1 demonstrate that only changes in moulin shape around h_{eq} affect the head and subglacial channel size. We use two different approaches to vary moulin shape near h_{eq} . In the first approach, we vary the moulin wall slope around h_{eq} (hourglass, diamond, Figure 1e,f) to keep our focus on the wall slope and not on the change in cross-sectional area at h_{eq} . In the second approach, we abruptly change the moulin cross-sectional area at h_{eq} (goblet, bottle, Figure 1g,h) to mimic differential ice melting (e.g. due to waterfall dynamics or heterogeneous ice properties) observed in moulins in the field (Covington et al., 2020). We compare results from all of these runs to the cylindrical standard, for a total of five moulin shapes.

As noted in Section 3.1, moulin shapes do not have a strong influence on dynamic timescales for a fixed $A_r(h_{\text{eq}})$; however, moulin shape does affect the amplitude and shape of the peaks and troughs in head and subglacial channel cross-sectional area in response to oscillating meltwater input. In this simulation set, we observe how the five tested shapes affect the amplitude and shape of the oscillating responses in h and S for the same sinusoidal meltwater input.

We compare cylindrical moulins, with radii varying from 3.5 – 15 m (Figure 4a–e), to hourglass- and diamond-shaped moulins with different wall slopes but with a common radius at one position in the moulin (Figure 4f–o), and to moulins with fixed wall slopes with varying radius (Figure 4p–y).

For similar Q_{in} , the oscillation amplitudes of h and S are controlled by the moulin volume within the oscillation range, similar to what was observed with a fixed input (Section 3.1). The magnitude of A_r in the head oscillation range, whether depth-independent (Figure 4a–e) or depth-varying (Figure 4f–y), strongly affects the amplitude of oscillations. For a given A_r at h_{eq} , a wall slope of just -2% from the vertical axis (Figure 4f–j red) can double the oscillation amplitude compared to a cylinder. This is due to the

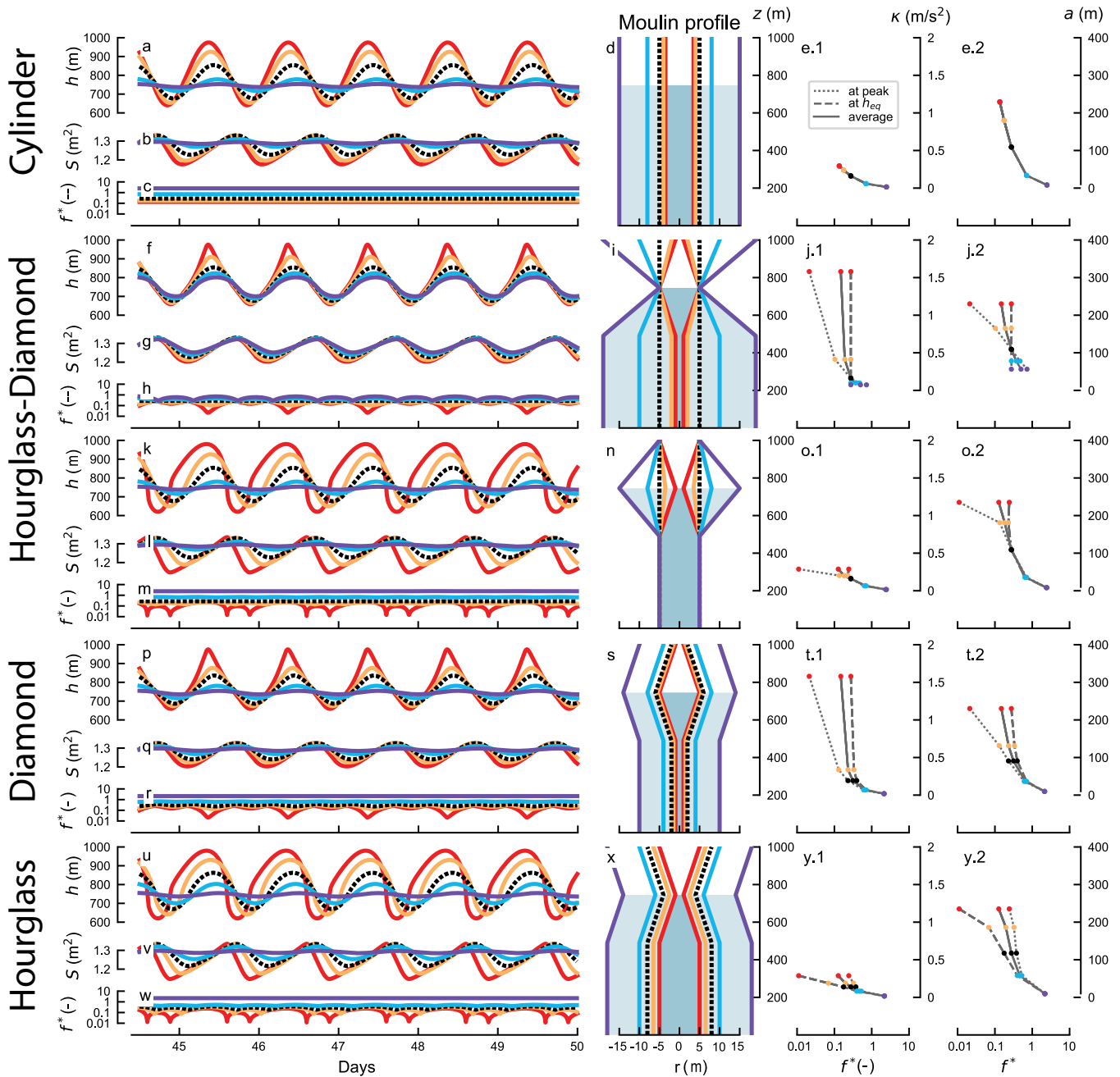


Figure 4. Timeseries of head (h), channel cross-sectional area (S), and dimensionless meltwater input frequency (f^*), for a sinusoidal Q_{in} oscillating from 2.6 to $3.4 \text{ m}^3\text{s}^{-1}$ with a daily period for multiple idealized moulin shapes. For cylindrical moulins (a–e) the radius (r) is uniform such that a large radius dampens oscillations in h and S , reducing f^* uniformly. For hourglass-diamond shaped moulins the radius is either fixed at h_{eq} , with varying wall slope above and below h_{eq} (f–j), or the radius is fixed above and below the water oscillation, and the radius varies at h_{eq} (k–o). For diamond-shaped (p–t) and hourglass-shaped (u–y) moulins the slope is fixed and the radius varies between model runs. Moulin profiles follow Fig (3). The correlation between peakedness, κ —represented by the second derivative of the head oscillation—and f^* (left) and the correlation between the peak-to-peak amplitude of oscillation (a) and f^* (right) are shown for each moulin shape. Values corresponding to peak head (dash-dot), equilibrium head (dashed), and mean values (solid) are shown.

depth-dependent moulin volume within the oscillation range: the ability of the moulin to store water decreases as h rises above h_{eq} , thus forcing a faster rise. This change in oscillation amplitude is particularly pronounced above the equilibrium head, where increases in radius at h_{eq} systematically reduce the amplitudes, regardless of the slope.

We observe asymmetry in both peak shape and the height of peaks versus depth of troughs above and below equilibrium. This asymmetry is driven by the asymmetry between the rates of melt and creep closure of the subglacial channel. In general, under conditions typical of an ice sheet, where the ice is thick, the subglacial channel is able to close faster than it can grow. This means that the subglacial channel closes quickly as meltwater input decreases and water pressure falls. But, when meltwater input increases, and the channel must reopen, the melt opening process is slower. Accordingly, the water level increases faster than the channel can accommodate, creating a large increase in water level in the moulin.

To investigate the relationship between moulin water level variation and moulin storage capacity, we use the dimensionless meltwater input frequency f^* from Covington et al. (2020), which is frequency of oscillation of the meltwater input nondimensionalized using a characteristic response timescale of moulin head:

$$f^* = \frac{\tau_{stor}}{P_{osc}}, \quad (8)$$

where the period of oscillation of the meltwater input (P_{osc}) is one day and the head response timescale, τ_{stor} , is defined as

$$\tau_{stor} = \left(\frac{\rho_i}{\rho_w} \right) \frac{H A_r}{Q_{in}}, \quad (9)$$

where ρ_i and ρ_w are the density of ice and water, respectively, H is the ice thickness, A_r is the moulin cross-sectional area, and Q_{in} is the meltwater input rate. Essentially, a moulin acts as a low-pass filter, where water storage filters out frequencies above $f^* \gtrsim 1$ in the resulting h and S dynamics, producing a filtered output Q_{out} (Covington et al., 2012). For the cylindrical case, where A_r is depth-independent, so too is f^* (Figure 4c). For non-cylindrical moulins, however, f^* changes with head (Figure 4h,m,r,w). For these cases, we use local cross-sectional area as a function of head, $A_r(h)$, to calculate f^* as a function of head.

For a cylindrical moulin, we find that when $f^* > 1$ (Figure 4a–e, purple line), diurnal oscillations are almost completely filtered out, but they remain for $f^* < 1$ (Figure 4c). For the diamond-shaped moulin (Figure 4r, yellow and red) the timeseries of f^* shows two pointy troughs per 24h period. The large and the small f^* troughs coincide with the peaks and troughs, respectively, of h , where A_r reaches minima. The main trough is due to the narrowing above h_{eq} , and the secondary trough is due to the narrowing below h_{eq} . Even though the moulin shape is symmetric above and below h_{eq} , the water level rises higher above h_{eq} than it falls below, due to the asymmetry caused by subglacial melt-creep dynamics. For the hourglass shaped moulin, the twice-daily troughs in f^* coincide with the subglacial channel cross-sectional extremum (Figure 4w). In this case, the narrowest portion of the moulin is positioned at h_{eq} .

We hypothesize that variations in oscillation shape (amplitude and peakedness) are controlled by the dimensionless meltwater input frequency (f^*). To quantify the peakedness (κ) of the oscillations, we calculate the curvature of the timeseries in the vicinity of the peak, using

$$\kappa = \left. \frac{d^2 h}{dt^2} \right|_{\text{peak}}, \quad (10)$$

411 where larger curvature values will correspond to a sharper peak. Finally, we calculate
412 the amplitude (a) of the oscillation above h_{eq} as

$$413 \quad a = h_{\text{peak}} - h_{\text{eq}}. \quad (11)$$

414 To test our hypothesis, we compare values of f^* at h_{eq} (dashed lines), h_{peak} (dotted-
415 dashed lines), and averaged (solid) against κ and a (Figure 4e,j,o,t,y). It is important
416 to keep in mind that for a specific H and Q_{in} , which here are held fixed, f^* is a direct
417 reflection of A_r . We find that the smallest value of f^* within the head oscillation range
418 controls the amplitude of oscillations if $f^* < 1$ (Figure 4), while the peakedness is controlled
419 by f^* averaged (Figure 4p-t, red line). Additionally, when the trough in f^* corresponds
420 to the equilibrium head (Figure 4h-y, red line), we observe deformation of the
421 head oscillation shape, but not a significant increase in κ . When the minimum values
422 of f^* coincide with a head maximum or minimum, the shapes of the peaks and troughs
423 become distorted. In other cases, when the troughs in f^* coincide with the water level
424 being at h_{eq} , then the shape distortion appears around the mean of the oscillation (Figure
425 4k-m, red line).

426 **3.3 Effect of abrupt change of moulin shape with constant and oscillating meltwater inputs** 427

428 Next we investigate how an abrupt change in moulin shape at a prescribed depth
429 affects the oscillation dynamics. Field exploration of moulins in Greenland (Covington
430 et al., 2020; Reynaud & Moreau, 1994; Moreau, 2009) has found ledges in some moulins,
431 or large subaerial volumes that narrow at the water line. To represent these moulins simply,
432 we design goblet and bottle-shaped moulins that comprise two stacked cylinders of
433 different radii (Figure 5f-j). We use these moulins to explore a hypothetical large change
434 in volume above h_{eq} or just below the lowest head (Figure 5k-o).

435 First, we test how the dynamic timescales are affected by an abrupt change in shape.
436 In contrast to the lack of impact of moulin wall slope (Figure 2g-i), we find that abrupt
437 enlargement or reduction of moulin size at h_{eq} substantially changes the oscillation and
438 damping timescales for the same meltwater input. We find that bottle-shaped moulins
439 have shorter damping timescales than cylindrical moulins, while hourglass-shaped moulins
440 require more time for the head to equilibrate (Supporting Figure S3).

441 We also test how this abrupt change in volume affects the head oscillations with
442 diurnally varying meltwater input (Figure 5). We find that abrupt changes in moulin radius
443 around h_{eq} affect the amplitudes of the oscillations in h and S . This is despite the
444 fact that all moulins had an identical radii for some 60% of the depth. An increase of
445 the moulin radius by just one meter (10%) reduced the amplitude of the water oscillations
446 by a third (Figure 5f-j, black and blue lines), suggesting that strongly dampened
447 water level oscillations can occur in moulins with a wide chamber above the water line,
448 regardless of their shape below the water line. In contrast, goblet and bottle-shaped moulins
449 in which the cylinders of different radii join below the oscillation range (Figure 5k-o) do
450 not show variations in the pattern or amplitude of water oscillation. These final simulations
451 illustrate that water level oscillations are insensitive to static storage volumes that
452 are always below the water level.

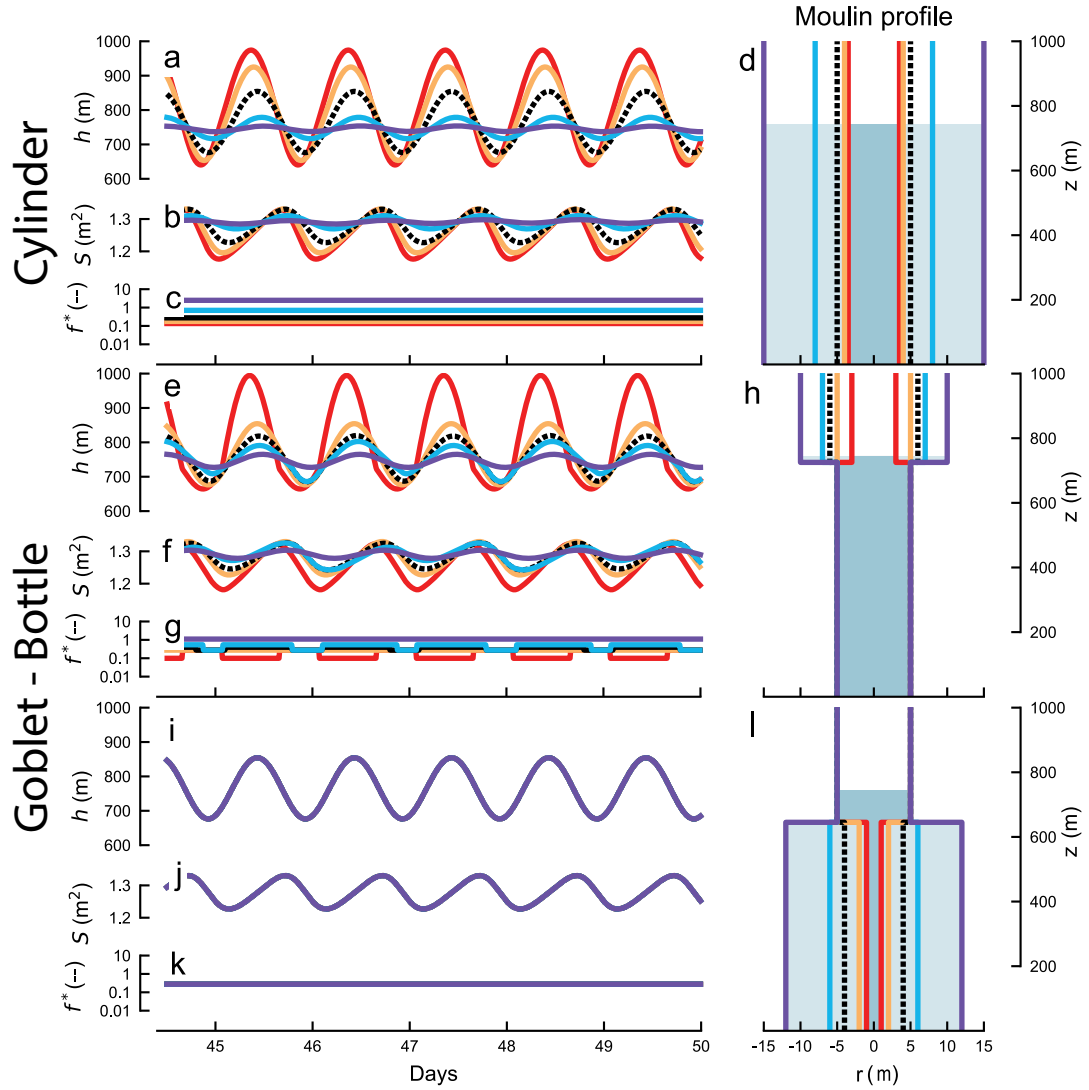


Figure 5. Timeseries of head (h), channel cross-sectional area (S), and dimensionless meltwater input frequency (f^*), for a daily sinusoidal Q_{in} oscillating from 2.6 to $3.4 \text{ m}^3 \text{ s}^{-1}$ for multiple idealized moulin shapes: Cylindrical (a-d), goblet-bottle-shaped with radius fixed below (e-h) and above (i-l) the equilibrium head (h_{eq}). The black dashed line represents the cylindrical moulin common to all the three simulation subsets.

4 Discussion

4.1 Controls on head variability

Moulin storage modulates changes in subglacial pressure by regulating variations in moulin hydraulic head (Andrews et al., 2022; Covington et al., 2012, 2020). Here, we examine how vertical changes in moulin storage impact the amplitude and form of moulin head oscillations. Moulins act as low-pass filters between meltwater inputs at the surface and englacial discharge into the subglacial system, removing high-frequency oscillations and transmitting low-frequency oscillations. This low-pass filter behavior can be quantified using the dimensionless oscillation frequency, f^* , where oscillations that occur on timescales where $f^* \gtrsim 1$ will be strongly damped.

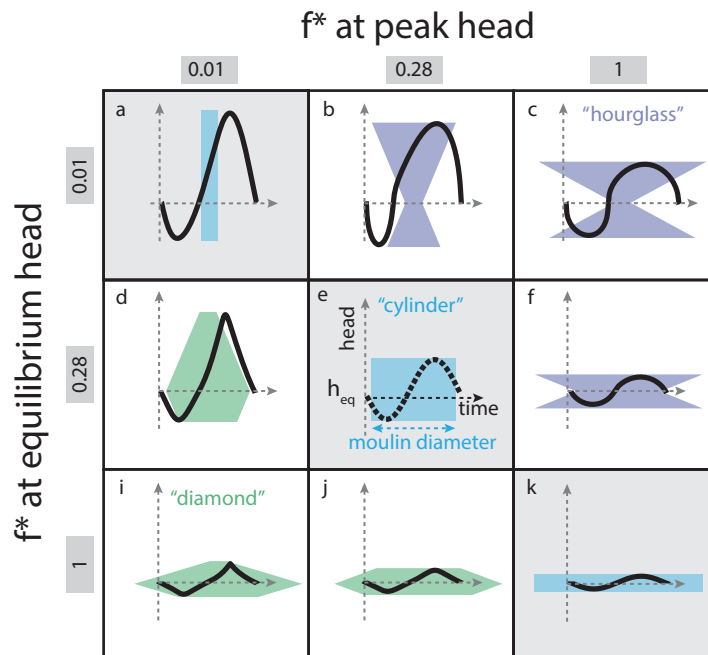


Figure 6. The amplitudes and shapes of moulin head (h) oscillations for selected dimensionless meltwater input frequency (f^*) at peak head (h_{peak}) and at equilibrium head (h_{eq}). Black lines show a single period of head oscillation. Green, blue, and purple shading shows the moulin shape within the range of water level oscillation for diamond-shaped, cylindrical, and hourglass-shaped moulins, respectively. Moulin shapes are scaled consistently against the head timeseries and with one another. All moulin shapes are symmetric about h_{eq} . Values of f^* are highlighted in grey.

The storage that impacts the head oscillations in the moulin is the storage within which the head varies. We define “dynamic storage” as the storage that fills and drains over the timescale of interest (generally a day or a season), and “static storage” as the storage that constantly contains water. Note storage that is static at the daily timescale could be dynamic at a longer timescale. The impact of dynamic storage on the water level patterns that we observe can be categorized using the values of f^* at the equilibrium head elevation, $f^*(h_{\text{eq}})$, and at the peak head elevation, $f^*(h_{\text{peak}})$. We generalize these patterns of behavior in Figure 6, where we display selected 24 h head oscillations for specific choices of $f^*(h_{\text{eq}})$ and $f^*(h_{\text{peak}})$.

472 Cylindrical moulin cases are depicted along the diagonal of Figure 6(a,e,k), where
 473 one can see the effect of increases in dimensionless meltwater input frequency leading to
 474 decreases in oscillation amplitude. However, oscillation amplitude also decreases if mov-
 475 ing along an axis of increasing $f^*(h_{\text{eq}})$ or increasing $f^*(h_{\text{peak}})$ (Figure 6b,c,f), suggest-
 476 ing that average f^* within the range of oscillation is responsible for controlling ampli-
 477 tude. The peakedness of moulin head oscillations is controlled by whether f^* decreases
 478 or increases as the water level approaches a peak or trough. Diamond-shaped moulins,
 479 which fall below the diagonal in Figure 6, and have $f^*(h_{\text{eq}}) > f^*(h_{\text{peak}})$, produce sharply
 480 peaked oscillations. Hourglass-shaped moulins, which are located above the diagonal in
 481 Figure 6, and have $f^*(h_{\text{eq}}) < f^*(h_{\text{peak}})$, produce rounded oscillations. For the diamond-
 482 shaped cases, cross-sectional area decreases towards the peaks and troughs. These de-
 483 creases in A_r drive an increase in the rate of change in head, leading to sharpening of
 484 the peaks. Similarly, if A_r increases towards peaks and troughs, then the rate of change
 485 in head will be reduced near peaks and troughs, producing rounded peaks. In addition
 486 to the low-pass filter behavior of moulins, changes in storage with depth can alter the
 487 temporal shapes of water level oscillations. Therefore, it may be possible to constrain
 488 the shapes of moulins by analyzing the shape of peaks and troughs in a timeseries of moulin
 489 water levels observed in the field.

490 4.2 Influence of model assumptions on simulation results

491 The simplification of the subglacial channel model to an ordinary differential equa-
 492 tion is based on the following assumptions: (1) that the hydraulic gradient is set by the
 493 large-scale topography of the ice sheet, which can be approximated by h/L , and (2) that
 494 changes in flow resistance are controlled by the cross-sectional area of the subglacial chan-
 495 nel near the moulin. The first assumption is based on the long and relatively flat topog-
 496 raphy of the ice sheet, and the fact that the hydraulic grade line within subglacial chan-
 497 nels tends to roughly follow the glacier topography (Röthlisberger, 1972). The second
 498 assumption is based on the idea that the largest flow resistance in the subglacial chan-
 499 nel will occur near the moulin, because the ice is thickest there and the creep closure timescale
 500 is the shortest. In fact, comparisons with our 1D model indicate that this second assump-
 501 tion produces channel cross-sectional areas in our 0D model that are within a few per-
 502 cent of the equivalent uniform pipe cross-sections that would produce the total head gra-
 503 dients in our 1D model runs (Supporting Figure S7). In the natural system, downstream
 504 increases in discharge will also tend to increase channel cross-sections and further reduce
 505 flow resistance downstream, such that our model is mostly likely to be representative of
 506 conditions near the moulin. In a recent lake drainage modeling study, Stubblefield et al.
 507 (2019) demonstrated that the usage of simplified coupled ordinary differential equations
 508 (ODEs), similar to the ones we use, instead of more complex partial differential equa-
 509 tions (PDEs), is sufficient for simulating upstream pressure dynamics in the vicinity of
 510 the moulin, while saving considerable computing time and reducing parameter complex-
 511 ity.

512 We also compared the outputs from a more complex PDE model, where the chan-
 513 nel can evolve along the horizontal axis, against our lumped ODE model (Supporting
 514 Text S3 and Figure S6). While a more thorough investigation on how subglacial water
 515 pressure evolves along a subglacial channel would be interesting in the future, we found
 516 that using the more complex model did not significantly change the water level dynam-
 517 ics at the moulin; head amplitude difference between the two simulation outputs are about
 518 5% of the ice thickness. However, the mean water level is somewhat different in the two
 519 simulations, a result of the simplifying assumptions in our ODE model. In the ODE model,
 520 the hydraulic gradient is a bit steeper than it would be in reality, effectively increasing
 521 the flow for a given hydraulic head and channel cross-sectional area, S . On the other hand,
 522 the average S is underestimated, as we use a value representative of where the ice thick-
 523 ness is the largest. In reality, we expect S to increase as the ice thickness decreases along
 524 the channel toward the margin, due to lower creep-closure rates under thinner ice. The

525 smaller S in our ODE model would effectively decrease flow for a given hydraulic head,
526 somewhat countering the influence of the other assumption. However, these two effects
527 do not quite balance, resulting in the slight differences in mean head values in the dis-
528 cretized (PDE) and lumped (ODE) channel models. However, as we are interested in the
529 relative change in water level induced by different moulin shapes, rather than the ab-
530 solute head values, the simplified representation of the subglacial channel in our model
531 does not have a substantial influence on our conclusions.

532 A second important simplification of the model is that it does not have a distributed
533 network, which in reality would likely exchange water with the subglacial channel. We
534 might expect such exchange flows with a distributed network to reduce the amplitude
535 of oscillation of the head in the moulin. However, observed water levels in moulins in Green-
536 land rarely reach pressures observed in the unchanneled portion (Andrews et al., 2014;
537 Covington et al., 2020; Mejia et al., 2021; Meierbachtol et al., 2013; Wright et al., 2016),
538 which is necessary for the water to be pushed into the distributed network. Furthermore,
539 daily changes in storage volumes within the distributed network are limited, again sug-
540 gesting that they would not have a substantial impact on moulin water level dynamics
541 (Covington et al., 2020).

542 Arguably, one of the most limiting assumptions in our model is its representation
543 of the englacial–subglacial system as a single moulin connected to a single channel, rather
544 than a network. In reality, moulins will interact with other nearby moulins, such that
545 the shape of a single moulin will not be the only driving factor of head variation (Andrews
546 et al., 2014, 2022). Moulin water level dynamics will likely average over storage avail-
547 able in nearby moulins that are tightly coupled through the channel network. Addition-
548 ally, there may be background discharge from other moulins or basal melt that could pro-
549 vide a baseflow discharge; this would reduce the head oscillation amplitude (Andrews
550 et al., 2022; Trunz, 2021). While such effects are likely to influence moulin water level
551 dynamics in nature, they are largely independent of moulin shape. Thus, the model pre-
552 sented here is sufficient to explore the relative impact of moulin shape on water level os-
553 cillations.

554 4.3 Potential shapes of Greenland Ice Sheet moulins

555 Here we have used idealized shapes to explore, in general, how moulin shape can
556 influence subglacial water pressure dynamics. We tested a range of cases, including ex-
557 treme end-members; however, real-world moulins are likely to display a somewhat nar-
558 rower range of shapes than we tested. In general, moulins will evolve through a combi-
559 nation of melt due to turbulent flow of water and viscous and elastic deformation of the
560 ice (Andrews et al., 2022; Catania & Neumann, 2010; Poinar et al., 2017). Recent model
561 experiments suggest that moulin shape evolves relatively quickly (days to weeks) within
562 a melt season to a near-equilibrium, with diurnally forced oscillations superimposed (Andrews
563 et al., 2022). Hence, the size of a moulin should be correlated to the size of the supraglacial
564 stream feeding it. This likely restricts plausible ranges of f^* , which depends linearly on
565 moulin volume and inversely on meltwater discharge.

566 The limited field observations inside the Greenland Ice Sheet (Covington et al., 2020;
567 Reynaud & Moreau, 1994) have not yet extended beyond the upper 10–20% of the ice
568 thickness, because moulins have been water-filled below that depth at the time of ex-
569 ploration. Water levels in the fall, when lower rates of stream flow make exploration pos-
570 sible, may also be somewhat higher than average summer water levels due to creep clo-
571 sure. This would modify the geometry, generally making a moulin narrower. Some ob-
572 served moulins also have ranges of water level oscillation that are much larger than the
573 explored thicknesses (Andrews et al., 2014), highlighting additional uncertainty on moulin
574 shapes within the relevant range of water level oscillations. Nevertheless, observations
575 in the upper parts of moulins suggest that goblet shapes may be more plausible than bot-

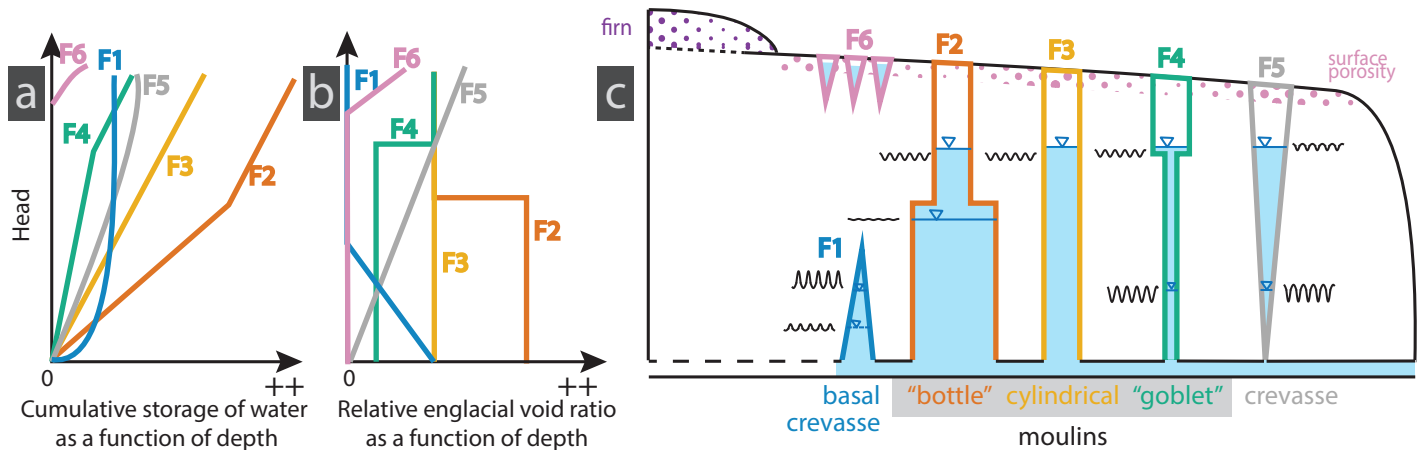


Figure 7. Conceptual sketch of englacial storage and relative englacial void ratio as a function of depth for idealized moulin shapes and for a similar volume of surrounding ice, or moulin density. The total stored water (a) gradually increases with increases in head, while the relative englacial void ratio (b) only changes when the radius of the moulin changes. (c) Representations of moulin profiles plotted in (a) and (b). Black oscillating timeseries depict the amplitude of water level oscillations in moulins when the water is at a specific depth. Oscillation amplitude is not a function of total moulin/englacial storage, but the dynamic storage, which is localized within the range of head oscillation.

576 the shapes. Some explored moulins are roughly cylindrical with a reduction of diameter
 577 at the water line, as observed in a moulin nearby the FOXX drill site (monitored by Andrews
 578 et al. (2014) and explored by Covington et al. (2020)) and in the Isortoq moulin (Reynaud
 579 & Moreau, 1994). The Phobos moulin was also goblet-shaped, with a large chamber just
 580 above the water level (Covington et al., 2020). We use the bottle shape moulin here as
 581 an end-member case to understand how head dynamics relate to moulin shape, but it
 582 is unclear what physical processes could produce such a shape. Phobos moulin did nar-
 583 row substantially within 50 meters of the ice surface, but it is doubtful that water lev-
 584 els would ever reach that elevation because the water level measured in the instrumented
 585 moulin nearby remained below 225 meters depth (Covington et al., 2020) throughout
 586 the 2017 melt season.

587 Goblet-shaped moulins could be produced by differential melting of the walls, with
 588 more melt above the equilibrium water level than below, or by strong creep closure of
 589 the ice at depth (Andrews et al., 2022). Field observations show that moulins tend to
 590 form in pre-existing crevasses, lake-drainage-induced fractures, or shear fractures (King,
 591 2018; Das et al., 2008; Smith et al., 2015). Such crevasses or fractures could also create
 592 zones of preferential melt, wherein waterfall erosion processes and supraglacial stream
 593 knickpoints could more rapidly enlarge moulin cross-sections. Because creep closure is
 594 relatively slow in the top 100 meters of an ice column, these goblet shapes should tend
 595 to be available for reuse from year to year (Catania et al., 2008). It is unclear if newly
 596 formed moulins provide more storage than reused moulins, as a reused moulin should
 597 partially creep closed over winter. More field observations and modeling are necessary
 598 to fully understand the processes that control moulin shapes.

4.4 Implications for large-scale glacier hydrological models

To more accurately simulate subglacial pressure amplitudes in the efficient portion of the subglacial drainage system, subglacial hydrological models often use an englacial void parameter. The englacial void parameter accounts for the transient storage of water in the englacial system (Flowers & Clarke, 2002). Englacial storage of water connected to the bed will influence the amplitude and the timing of peak subglacial water pressure. Moulins may be the most important englacial storage component, as they are directly connected to both the subglacial and supraglacial channels; limited data also suggest that storage from moulins is plausibly of the same order of magnitude as storage values normally used in models (Covington et al., 2020). The englacial void ratio or englacial void fraction parameter is typically calculated as the volume of void space divided by the bulk volume of the glacier (Downs et al., 2018; De Fleurian et al., 2018; Flowers, 2015). Although overall storage in the glacier is important on longer timescales, we find that it is only the storage or englacial void ratio within the head oscillation range, which we call the dynamic storage, that affects the water level dynamics in the efficient portion of the bed on a daily timescale.

As we find that the head oscillation amplitudes are strongly affected by dynamic storage, we reflect here on the extent to which different types of englacial storage contribute to this dynamic storage. We compare five shapes to illustrate how total water storage and local englacial storage vary with depth (Figure 7, englacial storage elements are numbered from F1 to F6). Moulins sketched in Figure 7(F2–F4) show that even though they have very different total storage capacities, they could induce similar head oscillation ranges if the water level is close to their tops (upper sinusoids). In the case of much lower water levels, though, the moulins would create very different oscillations (lower sinusoids). The high dynamic storage in moulin F2 will dampen oscillations, whereas the low dynamic storage in moulin F4 will enable large oscillations. Crevasses (Figure 7-F5) connected to a moulin could provide a substantial extra volume that could dampen oscillation amplitudes and filter out high-frequency variations (Colgan et al., 2011). Without such a connection, crevasses could provide long term storage at seasonal timescales (McGrath et al., 2011). Basal crevasses (Figure 7-F1), if they are connected to the channelized system, would only influence the oscillation dynamics if the water level oscillated within the crevasse. Basal crevasses have been found in drilling (Harper et al., 2010) and seem to be present when basal water pressures are above overburden pressure (van der Veen, 1998). Therefore, they may be more likely in the weakly connected portion of the bed that has higher water pressure than the channelized system (Andrews et al., 2014; Wright et al., 2016). The firn aquifer, the surface crevasses, and the porosity at the surface (F6), while capable of delaying the arrival of meltwater to the moulin, are storage elements that are completely decoupled from basal water pressure, as they are not typically directly connected with the subglacial hydrological system (Downs et al., 2018; Hewitt, 2013). Thus, while we include them in Figure 7 for completeness, they should have no role in the dynamic storage that we posit influences the englacial void ratio.

Models typically treat storage as homogeneous, and therefore independent of vertical position (Banwell et al., 2016; Flowers & Clarke, 2002; Flowers, 2015; De Fleurian et al., 2018). However, water storage is a function of depth (Figure 7). We find that the storage volume, or englacial void, that will affect basal water pressure dynamics in the channelized and surrounding distributed portions of the bed is the volume of moulins and connected crevasses within the range of head variation. The equilibrium head h_{eq} in a moulin (Meierbachtol et al., 2013; Röthlisberger, 1972), which is not influenced by the moulin shape but by the glacier characteristics (e.g. ice thickness, subglacial channel length) and the rate of discharge, can be predicted and is shown in Supporting Figure S4 for a wide range of mean meltwater inputs. The size and shape of the storage volume near equilibrium head, which is expected to be up to a few hundreds of meters below the surface, likely controls the amplitude and shape of daily head oscillation and has

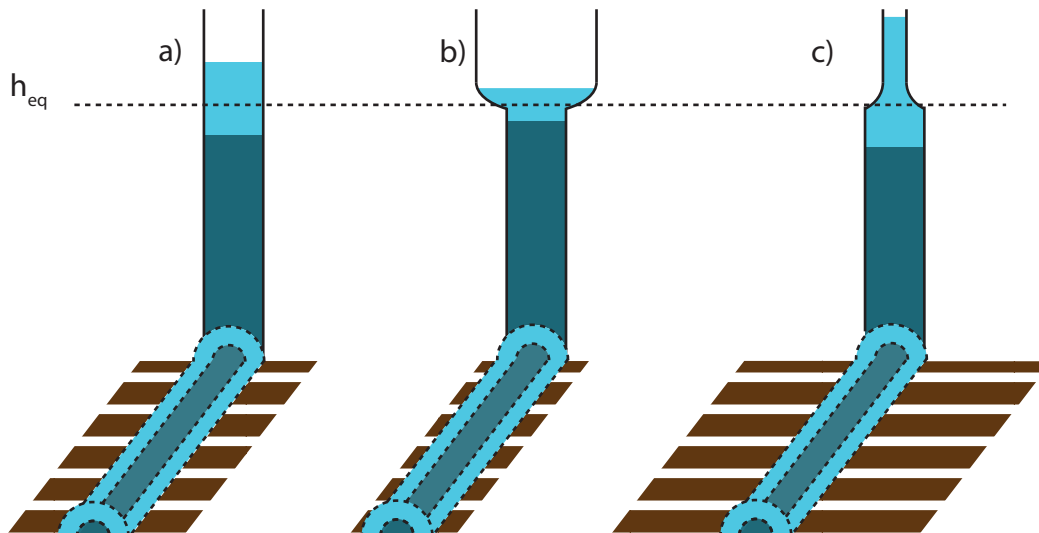


Figure 8. A comparison of the oscillation range for three example moulin shapes and the potential impact on the weakly connected portion of the bed. Light and dark blue indicate the ranges of oscillation in moulin water level and cross-sectional area of the subglacial channel. The brown striations represent the spatial range of influence of the moulin over the surrounding weakly connected bed, with larger pressure oscillations leading to a larger area of influence.

652 the ability to filter out meltwater variability with sufficiently high frequency ($f^* \gtrsim 1$).
 653 Because moulins are directly connected to the efficient channelized system, the dynamic
 654 portion of the moulin may represent a substantial percentage of the englacial void ratio
 655 ratio used in subglacial hydrology models.

656 4.5 The impact of moulin shape on subglacial connectivity and ice speed

657 While this study investigates how moulin shape modulates water pressures within
 658 idealized subglacial channels, we use our results to speculate on how moulin shape might
 659 influence sliding speeds on seasonal timescales. Observed late-melt-season slowdowns have
 660 been attributed to the dewatering of isolated or weakly connected cavities (Andrews et
 661 al., 2014; Hoffman et al., 2016) Here, we consider the potential role of moulin shape in
 662 this dewatering process by comparing goblet and bottle-shaped moulins to the standard
 663 cylindrical shape (Figure 8), which all have the same radius at the equilibrium head h_{eq} .

664 When compared to a cylindrical moulin (Figure 8a), a goblet-shaped moulin (which
 665 exploration suggest are more common) with the same radius at and below the equilib-
 666 rium head (Figure 8b) will have smaller diurnal water level oscillations, whereas a bottle-
 667 shaped moulin (Figure 8c) will have larger oscillations. Larger amplitude water level os-
 668 cillations should induce stronger subglacial water pressure gradients, forcing water fur-
 669 ther out into the neighboring distributed drainage system. This could potentially lower
 670 pressures within a larger number of weakly connected cavities and connect a larger por-
 671 tion of the surrounding distributed system (Figure 8c). On the other hand, a moulin with
 672 smaller oscillations would have less ability to grow connectivity within the surrounding
 673 bed.

674 As long-term ice velocities are thought to relate to the weakly connected
 675 portion of the bed, short-term pressure variability may play an important part in determining
 676 whether early melt season increases in sliding speeds are offset by slowdowns later in the
 677 melt season. Our results show that moulin shape and size influence pressure variability.

678 To offer stronger constraints on the impact of moulin over ice-sheet scales, more infor-
679 mation is needed on the sizes and shapes of moulins and whether they differ systemat-
680 ically across the ice sheet.

681 **4.6 Complementary approaches to constraining the role of moulins in** 682 **ice-sheet hydrology**

683 We have shown that damping timescales, oscillation amplitude and shape, as well
684 as short-term englacial storage are affected only by volume and changes in volume with
685 height within the head oscillation range. Therefore, characterizing the shapes of the up-
686 per portions of moulins will provide constraints for model storage parameters and aid
687 in interpretation of field data.

688 In order to appropriately represent the englacial storage directly connected to the
689 subglacial channel system, one must determine not only the moulin density and distri-
690 bution, which can be estimated from satellite imagery (Phillips et al., 2011; Smith et al.,
691 2015), but also the geometry of moulins below the surface. If non-cylindrical moulins are
692 prevalent, it may not be possible to infer the cross-sectional areas of moulins relevant
693 for dynamic storage from satellite imagery, or even from surface observations, since vol-
694 umes at depth may be very different than those observed at the surface. Moulin explo-
695 ration is difficult, but continued mapping of moulins could provide precious data to con-
696 strain the plausible range of dynamic storage volumes within the Greenland Ice Sheet.
697 While exploration and mapping of moulins will provide needed initial information on the
698 typical sizes and shapes of moulins and the factors that influence them, the resources
699 needed for such exploration will limit the number of moulins that can be mapped. There-
700 fore, it is also necessary to understand the processes that lead to the creation of differ-
701 ent shapes by modeling of moulin evolution. In this study, we simulated water level within
702 moulins with a static shape. The time evolution and lifetimes of moulins will also likely
703 influence how moulins modulate subglacial water pressures. A physically based model
704 for moulin evolution, informed by field observations from moulin exploration, could pro-
705 vide the information needed to extrapolate dynamic storage volumes across the ice sheet
706 scale.

707 Finally, the model we use represents a single moulin connected to a single chan-
708 nel. In reality, moulins are connected to a network of subglacial channels, exchanging
709 and regulating meltwater inputs with one another. Therefore, understanding how a com-
710 plex network of moulins interacts will be necessary to get a full picture of the impact of
711 moulins on subglacial pressures. Since prior observations of nearby moulin water levels
712 suggest rapid equilibration of heads through the subglacial system (Andrews et al., 2014),
713 it seems likely that the dynamic storage governing water pressure variability represents
714 an areally-averaged storage volume across many coupled moulins within a region of the
715 ice sheet.

716 **5 Conclusion**

717 We use a simplified model of a subglacial channel coupled to a moulin to explore
718 relationships between moulin shape and head variation. Our results show that the shape
719 of the moulin within the range of water level oscillations is the main control on the tem-
720 poral pattern of head dynamics. More specifically, the size of the moulin at and around
721 the equilibrium head position controls the amplitude of the oscillations, while the shape
722 of the moulin controls the shape of the peaks and troughs in water level as a function
723 of time. For subglacial hydrological models to appropriately capture pressure dynam-
724 ics, storage parameters, such as the englacial void ratio, must quantify dynamic storage,
725 which fills and drains, rather than total static storage. Given their direct connectivity
726 to the subglacial system and potentially large volume at depth, moulins may represent
727 an important percentage of the dynamic storage. To quantify this dynamic storage within

728 moulins, we need better constraints on both moulin shape near the water level h_{eq} and
729 moulin density. Previous work has demonstrated that moulin cross-sections at the ice
730 surface are not necessarily representative of cross-sections at depth, suggesting the rel-
731 ative difficulty of making this measurement.

732 In addition, we find that the dynamic storage of moulins dictates the magnitude
733 of subglacial pressure increases associated with short-term perturbations in supraglacial
734 runoff. The presence of large voids just above the equilibrium head position can strongly
735 dampen the head oscillation amplitudes, even if the rest of the moulin has a relatively
736 small diameter. Such small-amplitude oscillations in pressure may inhibit the growth of
737 connectivity within the surrounding weakly connected bed and potentially reduce the
738 mid-to-late-season ice sheet slow down caused by sustained large meltwater inputs to the
739 bed. Future modeling or mapping of moulins would enable better constraints on real-
740 istic ranges for dynamic storage within moulins and the controls on that storage, and
741 therefore would improve understanding of the impact of meltwater on ice motion.

742 **Notation**

743 a Amplitude of the moulin head oscillation above h_{eq} [L]
744 A_r Moulin cross-sectional area [L]
745 $A_r(h)$ Moulin cross-sectional area at the water level [L]
746 f^* Non-dimensional meltwater input frequency [-]
747 H Ice thickness [L]
748 h Moulin hydraulic head [L]
749 h_{eq} Moulin equilibrium hydraulic head [L]
750 κ Peakedness of the moulin head oscillation in the vicinity of the peak [LT^{-2}]
751 L Subglacial channel length [L]
752 m Moulin wall slope $\Delta r/\Delta z$ [-]
753 Q_a Amplitude of oscillation of the meltwater input [L]
754 Q_{in} Supraglacial meltwater input [L^3T^{-1}]
755 Q_{mean} Mean meltwater input [L^3T^{-1}]
756 Q_{out} Subglacial channel water output [L^3T^{-1}]
757 r Moulin radius [L]
758 r_{base} Moulin radius at the base of the moulin [L]
759 r_{heq} Moulin radius at equilibrium head [L]
760 r_{top} Moulin radius at the top of the moulin [L]
761 S Subglacial channel cross-sectional area [L^2]
762 t Time [T]
763 τ_{damp} Damping timescale [T]
764 τ_{osc} Period of oscillation timescale [T]
765 z Elevation from bedrock [L]

766 **6 Open Research**

767 The code (in Python) used to make the simulations and create the figures is avail-
768 able in a public Github repository. The current version of the model repository is the
769 Release v.4 (Trunz & Covington, 2022) and is available here: [https://zenodo.org/record/](https://zenodo.org/record/6841708)
770 [6841708](https://zenodo.org/record/6841708).

771 **Acknowledgments**

772 C.T., M.D.C., J.M., and J.G. were supported by the United States National Science Foun-
773 dation grants 1604022. K.P. and L.C.A. received support from NASA Cryosphere award
774 80NSSC19K0054. The authors declare there are no conflicts of interest with regard to
775 finances or with the results of this paper.

776 **References**

- 777 Andrews, L. C., Catania, G. A., Hoffman, M., Gulley, J., Lüthi, M. P., Ryser, C.,
778 ... Neumann, T. A. (2014). Direct observations of evolving subglacial
779 drainage beneath the Greenland Ice Sheet. *Nature*, 514(7520), 80–83. doi:
780 10.1038/nature13796
781 Andrews, L. C., Poinar, K., & Trunz, C. (2022). Controls on Greenland moulin ge-
782 ometry and evolution from the Moulin Shape model. *The Cryosphere Discus-*
783 *sions*, 1–47. (accepted) doi: 10.5194/tc-2021-41
784 Arnold, N., Richards, K., Willis, I., & Sharp, M. (1998). Initial results from a dis-
785 tributed, physically based model of glacier hydrology. *Hydrological Processes*,
786 12(2), 191–219.
787 Banwell, A., Hewitt, I., Willis, I., & Arnold, N. (2016). Moulin density controls

- 788 drainage development beneath the Greenland ice sheet. *Journal of Geophysical*
789 *Research: Earth Surface*, 121(12), 2248–2269. doi: 10.1002/2015JF003801
- 790 Bartholomew, T. C., Anderson, R. S., & Anderson, S. P. (2011). Growth and
791 collapse of the distributed subglacial hydrologic system of Kennicott Glacier,
792 Alaska, USA, and its effects on basal motion. *Journal of Glaciology*, 57(206),
793 985–1002. doi: 10.3189/002214311798843269
- 794 Bartholomew, I., Nienow, P., Sole, A., Mair, D., Cowton, T., & King, M. A. (2012).
795 Short-term variability in Greenland Ice Sheet motion forced by time-varying
796 meltwater drainage: Implications for the relationship between subglacial
797 drainage system behavior and ice velocity. *Journal of Geophysical Research:*
798 *Earth Surface*, 117(3), F03002. doi: 10.1029/2011JF002220
- 799 Bourseiller, P., Lambertson, J., Moreau, L., Couté, A., & Quennehen, C. (2002). *Voy-*
800 *age dans les glaces*. Paris: La Martinière Jeunesse.
- 801 Catania, G. A., & Neumann, T. A. (2010). Persistent englacial drainage features in
802 the Greenland Ice Sheet. *Geophysical Research Letters*, 37(2), L02501. doi: 10
803 .1029/2009GL041108
- 804 Catania, G. A., Neumann, T. A., & Price, S. F. (2008). Characterizing englacial
805 drainage in the ablation zone of the Greenland ice sheet. *Journal of Glaciol-*
806 *ogy*, 54(187), 567–578. doi: 10.3189/002214308786570854
- 807 Clarke, G. K. C. (1996). Lumped-element analysis of subglacial hydraulic circuits.
808 *Journal of Geophysical Research: Solid Earth*, 101(B8), 17547–17559. doi: 10
809 .1029/96JB01508
- 810 Colgan, W., Steffen, K., McLamb, W. S., Abdalati, W., Rajaram, H., Motyka, R.,
811 ... Anderson, R. (2011). An increase in crevasse extent, West Greenland:
812 Hydrologic implications. *Geophysical Research Letters*, 38(18), L18502. doi:
813 10.1029/2011GL048491
- 814 Covington, M. D., Banwell, A., Gulley, J., Saar, M. O., Willis, I., & Wicks, C. M.
815 (2012). Quantifying the effects of glacier conduit geometry and recharge
816 on proglacial hydrograph form. *Journal of Hydrology*, 414, 59–71. doi:
817 10.1016/j.jhydrol.2011.10.027
- 818 Covington, M. D., Gulley, J. D., Trunz, C., Mejia, J., & Gadd, W. (2020). Moulin
819 Volumes Regulate Subglacial Water Pressure on the Greenland Ice Sheet. *Geo-*
820 *physical Research Letters*, 47(20). doi: 10.1029/2020GL088901
- 821 Covington, M. D., Wicks, C. M., & Saar, M. O. (2009). A dimensionless num-
822 ber describing the effects of recharge and geometry on discharge from sim-
823 ple karstic aquifers. *Water Resources Research*, 45(11), W11410. doi:
824 10.1029/2009WR008004
- 825 Cowton, T., Nienow, P., Sole, A., Bartholomew, I., & Mair, D. (2016). Variabil-
826 ity in ice motion at a land-terminating Greenlandic outlet glacier: the role of
827 channelized and distributed drainage systems. *Journal of Glaciology*, 62(233),
828 451–466. doi: 10.1017/jog.2016.36
- 829 Das, S. B., Joughin, I., Behn, M. D., Howat, I. M., King, M. A., Lizarralde, D., &
830 Bhatia, M. P. (2008). Fracture Propagation to the Base of the Greenland Ice
831 Sheet During Supraglacial Lake Drainage. *Science*, 320(5877), 778–781. doi:
832 10.1126/science.1153360
- 833 De Fleurian, B., Werder, M. A., Beyer, S., Brinkerhoff, D. J., Delaney, I., Dow,
834 C. F., ... Sommers, A. N. (2018). SHMIP The subglacial hydrology model
835 intercomparison Project. *Journal of Glaciology*, 64(248), 897–916. doi:
836 10.1017/jog.2018.78
- 837 Dow, C. F., Kulesa, B., Rutt, I. C., Doyle, S. H., & Hubbard, A. (2014). Up-
838 per bounds on subglacial channel development for interior regions of the
839 Greenland ice sheet. *Journal of Glaciology*, 60(224), 1044–1052. doi:
840 10.3189/2014JoG14J093
- 841 Downs, J. Z., Johnson, J. V., Harper, J. T., Meierbachtol, T., & Werder, M. A.
842 (2018). Dynamic Hydraulic Conductivity Reconciles Mismatch Between Mod-

- 843 eled and Observed Winter Subglacial Water Pressure. *Journal of Geophysical*
844 *Research: Earth Surface*, 123(4), 818–836. doi: 10.1002/2017JF004522
- 845 Flowers, G. E. (2015). Modelling water flow under glaciers and ice sheets. *Proc. R.*
846 *Soc. A*, 471(2176), 20140907. doi: 10.1098/rspa.2014.0907
- 847 Flowers, G. E., & Clarke, G. K. C. (2002). A multicomponent coupled model of
848 glacier hydrology 1. Theory and synthetic examples. *Journal of Geophysical*
849 *Research: Solid Earth*, 107(B11), 2287. doi: 10.1029/2001JB001122
- 850 Griselin, M. (1995). *3e symposium international, cavités glaciaires et cryokarst en*
851 *régions polaires et de haute montagne: Chamonix-France, 1er-6 novembre 1994*
852 *: actes*. Presses Univ. Franche-Comté.
- 853 Gulley, J., Benn, D., Sreaton, E., & Martin, J. (2009). Mechanisms of englacial con-
854 duit formation and their implications for subglacial recharge. *Quaternary Sci-*
855 *ence Reviews*, 28(19-20), 1984–1999. doi: 10.1016/j.quascirev.2009.04.002
- 856 Gulley, J., Walthard, P., Martin, J., Banwell, A., Benn, D., & Catania, G. (2012).
857 Conduit roughness and dye-trace breakthrough curves: why slow velocity
858 and high dispersivity may not reflect flow in distributed systems. *Journal of*
859 *Glaciology*, 58(211), 915–925. doi: 10.3189/2012JoG11J115
- 860 Harper, J. T., Bradford, J. H., Humphrey, N. F., & Meierbachtol, T. W. (2010).
861 Vertical extension of the subglacial drainage system into basal crevasses. *Nature*
862 *; London*, 467(7315), 579–82. doi: 10.1038/nature09398
- 863 Hewitt, I. (2013). Seasonal changes in ice sheet motion due to melt water lubrication.
864 *Earth and Planetary Science Letters*, 371-372, 16–25. doi: 10.1016/j.epsl
865 .2013.04.022
- 866 Hewitt, I., Schoof, C., & Werder, M. A. (2012). Flotation and free surface flow in a
867 model for subglacial drainage. Part 2. Channel flow. *Journal of Fluid Mechan-*
868 *ics*, 702, 157–187. doi: 10.1017/jfm.2012.166
- 869 Hoffman, M., Andrews, L. C., Price, S. A., Catania, G. A., Neumann, T. A., Luthi,
870 M. P., ... Morriss, B. (2016). Greenland subglacial drainage evolution regu-
871 lated by weakly connected regions of the bed. *Nature Communications*,
872 7(13903). doi: 10.1038/ncomms13903
- 873 Holmlund, P. (1988). Internal Geometry and Evolution of Moulins, Stor-
874 glaciären, Sweden. *Journal of Glaciology*, 34(117), 242–248. doi: 10.1017/
875 S0022143000032305
- 876 King, L. A. (2018). *Identifying and characterizing the spatial variability of*
877 *supraglacial hydrological features on the western Greenland Ice Sheet* (Doc-
878 toral dissertation, University of British Columbia). doi: 10.14288/1.0372827
- 879 Koziol, C. P., & Arnold, N. (2018). Modelling seasonal meltwater forcing of the
880 velocity of land-terminating margins of the Greenland Ice Sheet. *Cryosphere*,
881 12(3), 971–991. doi: 10.5194/tc-12-971-2018
- 882 Lambertson, J. (2002). *Les moulins de glace: mémoires d'un glacionaute*. Paris:
883 Hoëbeke.
- 884 McGrath, D., Colgan, W., Steffen, K., Lauffenburger, P., & Balog, J. (2011). As-
885 sessing the summer water budget of a moulin basin in the Sermeq Avannarleq
886 ablation region, Greenland ice sheet. *Journal of Glaciology*, 57(205), 954–964.
887 doi: 10.3189/002214311798043735
- 888 Meierbachtol, T., Harper, J., & Humphrey, N. (2013). Basal Drainage System
889 Response to Increasing Surface Melt on the Greenland Ice Sheet. *Science*,
890 341(6147), 777–779. doi: 10.1126/science.1235905
- 891 Mejia, J. Z., Gulley, J. D., Trunz, C., Covington, M. D., Bartholomaeus, T. C., Xie,
892 S., & Dixon, T. H. (2021). Isolated Cavities Dominate Greenland Ice Sheet
893 Dynamic Response to Lake Drainage. *Geophysical Research Letters*, 48(19),
894 e2021GL094762. doi: 10.1029/2021GL094762
- 895 Moreau, L. (2009). L'exploration du cryokarst glaciaire et son intérêt scien-
896 tifique pour l'étude du drainage des eaux de fonte : porches, cavités, crevasses,
897 bédrières et moulins. *Collection EDYTEM. Cahiers de géographie*, 8(1), 163–

- 898 170. doi: 10.3406/edyte.2009.1083
- 899 Nye, J. F. (1976). Water Flow in Glaciers: Jökulhlaups, Tunnels and Veins. *Journal*
900 *of Glaciology*, 17(76), 181–207. doi: 10.3189/S002214300001354X
- 901 Phillips, T., Leyk, S., Rajaram, H., Colgan, W., Abdalati, W., McGrath, D., & Stef-
902 fen, K. (2011). Modeling moulin distribution on Sermeq Avannarleq glacier
903 using ASTER and WorldView imagery and fuzzy set theory. *Remote Sensing*
904 *of Environment*, 115(9), 2292–2301. doi: 10.1016/j.rse.2011.04.029
- 905 Poinar, K., Joughin, I., Lilien, D., Brucker, L., Kehrl, L., & Nowicki, S. (2017).
906 Drainage of Southeast Greenland Firn Aquifer Water through Crevasses to the
907 Bed. *Frontiers in Earth Science*, 5. doi: 10.3389/feart.2017.00005
- 908 Reynaud, L., & Moreau, L. (1994). Moulins glaciaires des glaciers tempérés et froids
909 de 1986 à 1994 (Mer de Glace et Groenland) : morphologie et techniques de
910 mesures de la déformation de la glace. Paris.
- 911 Röthlisberger, H. (1972). Water Pressure in Intra- and Subglacial Channels. *Journal*
912 *of Glaciology*, 11(62), 177–203. doi: 10.1017/S0022143000022188
- 913 Schoof, C. (2010). Ice-sheet acceleration driven by melt supply variability. *Nature*,
914 468(7325), 803–806. doi: 10.1038/nature09618
- 915 Smith, L. C., Chu, V. W., Yang, K., Gleason, C. J., Pitcher, L. H., Rennermalm,
916 A. K., ... Balog, J. (2015). Efficient meltwater drainage through supraglacial
917 streams and rivers on the southwest Greenland ice sheet. *PNAS*, 112(4),
918 1001–1006. doi: 10.1073/pnas.1413024112
- 919 Sommers, A., Rajaram, H., & Morlighem, M. (2018). SHAKTI Subglacial Hydrol-
920 ogy and Kinetic, Transient Interactions v1.0. *Geoscientific Model Development*,
921 11(7), 2955–2974. doi: 10.5194/gmd-11-2955-2018
- 922 Spring, U., & Hutter, K. (1981). Numerical studies of jökulhlaups. *Cold Regions Sci-*
923 *ence and Technology*, 4(3), 227–244.
- 924 Stevens, L. A., Hewitt, I. J., Das, S. B., & Behn, M. D. (2018). Relationship Be-
925 tween Greenland Ice Sheet Surface Speed and Modeled Effective Pressure.
926 *Journal of Geophysical Research: Earth Surface*, 123(9), 2258–2278. doi:
927 10.1029/2017JF004581
- 928 Stubblefield, A. G., Creyts, T. T., Kingslake, J., & Spiegelman, M. (2019). Model-
929 ing oscillations in connected glacial lakes. *Journal of Glaciology*, 65(253), 745
930 – 758. doi: 10.1017/jog.2019.46
- 931 Trunz, C. (2021). *Modeling and Measuring Water Level Fluctuations in the Green-*
932 *land Ice Sheet: How Moulin Life Cycle and Shape can Inform us on the Sub-*
933 *glacial Drainage System*. (Doctoral Thesis). University of Arkansas, Fayette-
934 ville.
- 935 Trunz, C., & Covington, M. D. (2022, May). *cctrunz/ModelRepo_moulinshapestoragepaper*.
936 Zenodo. (type: ComputationalNotebook) doi: 10.5281/zenodo.6574988
- 937 Vallot, J. (1898). Exploration des moulins de la Mer de Glace. *Annales de*
938 *l'Observatoire météorologique du Mont-Blanc*, 3(1), 183–193.
- 939 van der Veen, C. J. (1998). Fracture mechanics approach to penetration of bot-
940 tom crevasses on glaciers. *Cold Regions Science and Technology*, 27(3), 213–
941 223. doi: 10.1016/S0165-232X(98)00006-8
- 942 Vatne, G., & Irvine-Fynn, T. D. L. (2016). Morphological dynamics of an englacial
943 channel. *Hydrology and Earth System Sciences*, 20(7), 2947–2964. doi: 10
944 .5194/hess-20-2947-2016
- 945 Werder, M. A., Hewitt, I. J., Schoof, C., & Flowers, G. E. (2013). Modeling chan-
946 nelized and distributed subglacial drainage in two dimensions. *Journal of Geo-*
947 *physical Research: Earth Surface*, 118(4), 2140–2158. doi: 10.1002/jgrf.20146
- 948 Werder, M. A., Schuler, T. V., & Funk, M. (2010). Short term variations of tracer
949 transit speed on alpine glaciers. *The Cryosphere*, 4(3), 381–396. doi: 10.5194/
950 tc-4-381-2010
- 951 Wright, P. J., Harper, J. T., Humphrey, N. F., & Meierbachtol, T. W. (2016).
952 Measured basal water pressure variability of the western Greenland Ice Sheet:

953
954
955

Implications for hydraulic potential: Greenland Ice Sheet Basal Water Pressure. *Journal of Geophysical Research: Earth Surface*, 121(6), 1134–1147. doi: 10.1002/2016JF003819